Mineral. Deposita 23, 24–33 (1988)

MINERALIUM
DEPOSITA

Fluid inclusion study of Xihuashan tungsten deposit in the southern Jiangxi province, China

G. Giuliani[1], **Y. D. Li**[2], **and T. F. Sheng**[3]

[1] ORSTOM, Embaixada da França, CP 665, 70404 Brasilia DF, Brazil
[2] Jiangxi Bureau of Geology, Nanchang, Jiangxi, China
[3] Chinese Academy of Geological Sciences, Institute of Mineral Deposits, 26 Baiwanzhuang Road, Beijing, China

Abstract. The Xihuashan tungsten deposit is closely related to a small highly evolved granitic intrusion. The fluid phases associated with the wolframite-bearing quartz veins have been investigated using microthermometry and the Raman microprobe; they are highly variable in density and composition. The earlier fluids are low-density and low-salinity CO_2-bearing aqueous solutions circulating at temperatures up to 420 °C, and low-salinity (2–3 equiv. wt% NaCl) aqueous solutions without traces of CO_2 circulating at high temperatures 280°–400 °C) involved in a specific hydrothermal fracturing event; limited unmixing occurs at 380 °C and 200–100 bar in response to a sudden pressure drop. The second types of fluids related to deposition of idiomorphic drusy quartz are typical CO_2-bearing aqueous solutions with low salinity (2.5 equiv. wt% NaCl) homogenizing at low to moderate temperatures (180°–340 °C). The late fluids characterize the sulfide deposition stage; they are aqueous fluids with variable salinities homogenizing in the liquid phase between 100° and 275 °C. The Xihuashan hydrothermal evolution resulted from a discontinuous sequence of specific events occurring between 420° and 150 °C and during a continuous hydrothermal evolution of the system during cooling. The role played by the CO_2-rich fluids in the transport and deposition of tungsten in the hydrothermal environment is discussed.

The Xihuashan mine belongs to the Dayu mining district located in the southern part of the Jiangxi province (Fig. 1). This tungsten deposit represents the typical wolframite-bearing quartz vein type of the Nanling metallogenic province (Yan et al. 1980) related to Jurassic biotite granites (Yenshan granites). Hsu (1943) first described the different tungsten mines from southern Jiangxi; then, specific and scientific metallogenic works were undertaken by Chinese researchers and geologists from the Dayu mining district. The results were presented at different international congresses (Tokyo 1979; Nanchang 1981; Nanjing 1982) and edited by Ishihara and Takenouchy (1980) and Hepworth and Yu Hong Zhang (1982). Further works on Jiangxi granites and their associated mineralizations were published in Chinese journals (Lu et al. 1982; Wang et al. 1982; Wang 1984) or in occidental publications (Tanelli 1982; Lebel et al. 1984; Giuliani 1985; Maruejol and Cuney 1985).

In this paper the fluid phases associated with the wolframite-bearing quartz veins at different exploration levels in Xihuashan mine are investigated using microthermometric and Raman spectrometric analyses. The knowledge of the bulk composition and density of the different fluid phases encountered in the quartz allows the PVTX evolution of the complex aqueous hydrothermal solutions responsible for tungsten mineralization in Xihuashan deposit to be followed.

Geology

The Xihuashan tungsten deposit is located on the border of a granitic stock composed of four intrusives, chronologically called $\gamma_5^{2\mathrm{a}}$, $\gamma_5^{2\mathrm{b}}$, $\gamma_5^{2\mathrm{c}}$, $\gamma_5^{2\mathrm{e}}$ (Wu and Mei 1982), that cut arenaceous and argillaceous anchizonal Cambrian formations (Fig. 1). Granite emplacement induces a wide thermal contact-metamorphic aureole. The deposit is situated in $\gamma_5^{2\mathrm{a}}$ and $\gamma_5^{2\mathrm{b}}$, and the contact zone is marked by the development of a "stockscheider" or a sporadic fine-grained granite designated $\gamma_5^{2\mathrm{b}'}$. The Xihuashan tungsten vein deposit is a typical wolframite vein type which occurs over an area of 4.3 km². In this area 615 commercial ore veins have been found, mainly trending EW (some ENE-WSW) and dipping northward with 75°–90°. The veins are developed inside the granite mainly in $\gamma_5^{2\mathrm{a}}$, and they pinch out at the contact zone with Cambrian hornfels. The veins are commonly 50–60 cm wide; individual veins are generally about 500 m long but can attain 1,075 m (vein 2.99). They are commonly 200–400 m thick and the commercial mineralization extends for 100–200 m, sometimes up to 300 m. The mineralized veins usually show an echelon structure in the horizontal and vertical directions and are distributed in groups or clusters.

More than fifty minerals have been described from ore veins in the Xihuashan district. Among the main minerals we found wolframite, cassiterite, molybdenite, bismuthinite, and scheelite which characterize the four stages of mineralizations (Table 1); the gangue minerals are quartz, potash feldspar, beryl, helvite, dolomite, and calcite.

The mineral assemblage is very different from the top to bottom of individual veins. A vertical zoning is commonly observed and may be generalized as follows (Yan et al. 1980): In the upper part the minerals are cassiterite, topaz, and beryl, while wolframite, molybdenite, and bismuthinite are concentrated in the middle part. In the lower part, wolframite diminishes and sulfides increase. In

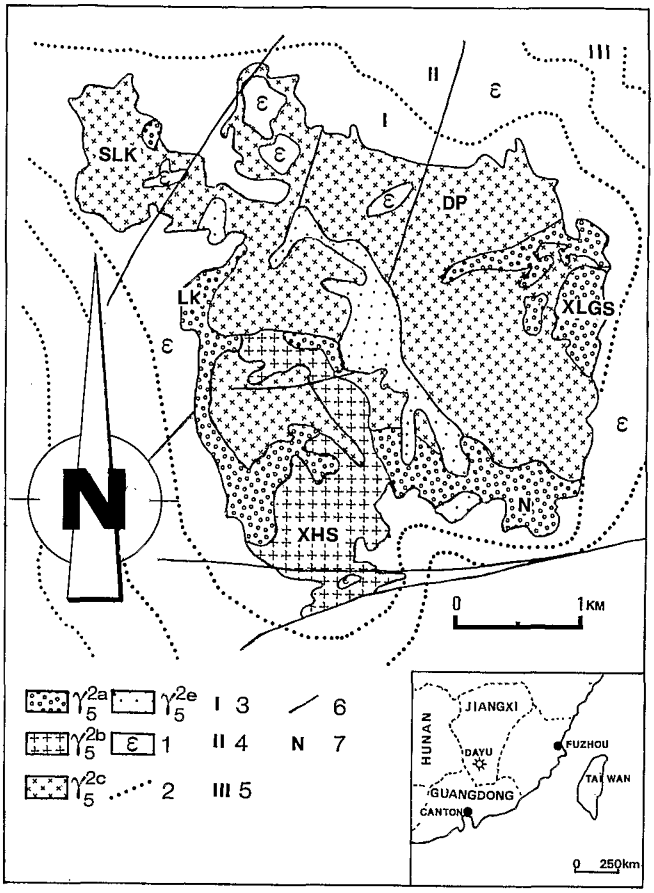

Fig. 1. Geological map of the Xihuashan granite stock with the main tungsten deposits. 1, metamorphic Cambrian series; 2, limit of the different metamorphic contact zones; 3, hornfels; 4, biotite-hornfels zone; 5, spotted schists; 6, faults; 7, main tungsten deposits; XHS, Xihuashan; LK, Laok'en; SLK, Sen Longko; DP, Dangping; XLGS, Xao Lsu Gshan; N, Niugushu

Table 1. Paragenesis of the main mineralized stages from the Xihuashan vein-type tungsten deposit

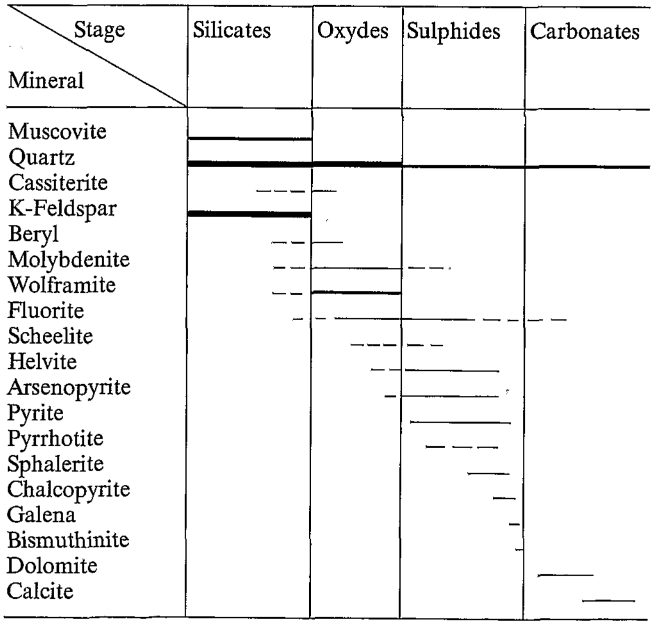

Stage / Mineral	Silicates	Oxydes	Sulphides	Carbonates
Muscovite	——			
Quartz	━━	━━	━━	━━
Cassiterite	- - -	—		
K-Feldspar	━━			
Beryl	- -	—		
Molybdenite	- -	——	- - -	
Wolframite	- -	——		
Fluorite	-	- ——	—— - -	- -
Scheelite		- - -	- -	
Helvite		- -	——	
Arsenopyrite		-	——	
Pyrite			——	
Pyrrhotite			- - -	
Sphalerite			——	
Chalcopyrite			—	
Galena			-	
Bismuthinite			-	
Dolomite				——
Calcite				——

the bottom part tin, tungsten, and beryllium minerals disappear and carbonates, fluorite, and sulfides develop. Scheelite is often the product of a secondary transformation of wolframite. Ore minerals are widespread in the vein following a rough lateral zonation (Yan et al. 1980) and the average grade of WO_3 in ore veins is about 1.08% for the whole deposit.

Samples and analytical techniques

Samples

For this fluid inclusion study representative samples of quartz were collected from several locations in the Xihuashan mine. Samples were taken mainly in vein 2.99 (the biggest vein at the mine) and vein 62, at the 632, 594, 538, and 431 levels; the last level corresponds to the bottom part of the vein 2.99. The vein quartz is massive, gray, and sometimes milky. Idiomorphic, transparent to cloudy crystals of quartz can be seen in vugs which are widespread in the veins. In fact, all quartz veins are fractured, and the healed fractures are infilled with several generations of quartz; this important fracturing reflects opening, rehealing, and successive fluid circulation and mineral deposition. So, the choice of samples, specifically for fluid inclusion study, was difficult.

Analytical techniques

For microthermometry fluid inclusions have been studied using the Chaix-Méca stage (Poty et al. 1976) that permits the temperature of phase transitions occurring in fluid inclusions during heating and cooling to be determined. Qualitative analysis of the solid phases observed in the inclusions was undertaken by electron microscopy with energy dispersive detectors.

For Raman spectrometry the nonaqueous part of the inclusion was analyzed with a Jobin-Yvon Raman microprobe type M.O.L.E. (Delhaye and Dhamelincourt 1975). Three gases were identified with their Raman lines, i.e., CH_4 (2,914 cm^{-1}), N_2 (2,330 cm^{-1}), and CO_2 (1,388 cm^{-1}). The area of each Raman line was measured with a planimeter with a precision of 1%. The mole fraction of each gas was calculated from the formulae listed in Dhamelincourt et al. (1979); the relative cross sections of Raman scattering are those given by Schrötter and Klöckner (1979), i.e., $CO_2 = 1.21$, $CH_4 = 9$, and $N_2 = 1$.

The principles for calculating the composition of these carbonic fluids (H_2O-CO_2-NaCl) have been presented by Ypma (1963), Poty et al. (1974), Touret (1976), and Burrus (1977) and recalculated for the H_2O-CO_2-NaCl-volatile system by Ramboz (1980) and Ramboz et al. (1985). The calculation is based on the knowledge of the composition and density of the aqueous fluid (microthermometric results and data from Potter and Brown 1977; Potter et al. 1978) and of the carbonic vapor at a temperature of < 31 °C (Raman probe and microthermometric data interpreted after Heyen et al. 1982). The bulk composition has been calculated considering the CO_2-CH_4-NaCl-H_2O system; the molar fraction of N_2 has been added to the molar fraction of CH_4, since there is at present insufficient knowledge of the theoretical systems CO_2-N_2-(CH_4) and especially CO_2-CH_4-N_2-NaCl-H_2O. Furthermore, CH_4 and N_2 have almost the same volatility and the systems

CO_2-CH_4-N_2 (Sarashina et al. 1971) and CO_2-CH_4 (Arai et al. 1971) are comparable (see Ramboz et al. 1985). Salinities were determined by clathrate melting and by the depression of freezing points due to the effect of dissolved CO_2 in the aqueous phase (Ellis and Golding 1963; Bozzo et al. 1973).

Analytical data

Microthermometry

Five main types of inclusions have been recognized in all samples (Table 2).

CO_2 type (type I). This less abundant type is found in samples from levels 632 and 594. These inclusions are widespread in the clean parts of quartz crystals. It is difficult to assess whether they have a primary or secondary character. The inclusions are about 12–15 µm in diameter sometimes with a negative crystal shape. They apparently do not have an aqueous phase. The microthermometric results are listed in Table 2: the CO_2 melting temperatures range from −58° to −56.6 °C, reflecting the presence of other volatile components (Donelly and Katz 1954); most of the inclusions homogenize in the gaseous phase at temperatures between 28° and 30 °C, but homogenization in the liquid phase occurs at 16.8 °C.

CO_2-H_2O type (type II). Three subtypes have been distinguished here.

Type-II A inclusions are three-phase, CO_2-rich inclusions with aqueous solution, liquid CO_2 (10–20 vol% of the cavity), and CO_2 vapor (50 vol% of the inclusion). They are observed in the levels 632, 594, and cometimes 538. This type occurs both as primary or secondary inclusions: some are located along crystallographic structures (e.g., the c-axis of quartz) sometimes associated with type I, but very often they are distributed along healed fracture planes or isolated in the quartz without any relationship to other inclusions. They have a negative crystal shape or are elongated and deformed showing the necking-down phenomena also with natural decrepitation. They are usually moderate in size (10–15 µm), but can be large (50 µm) when isolated; small solid opaque inclusions are common. The microthermometric features are summarized in Table 2: on heating, inclusions homogenize to both the liquid and the gas phases at temperatures ranging 300°–370 °C (Fig. 2).

Type-II B inclusions have been observed in all levels of Xihuashan mine. They contain an aqueous solution and a large gas bubble (40%–70% of the volume of the total inclusion). They are isolated in the quartz or clustered on healed fracture planes, sometimes being associated with type II A. Their shape is generally simple, occasionally with a negative crystal form; they are between 10 to 20 µm in diameter. The melting temperatures of CO_2 range from −56.9° to −58.5 °C and the liquid CO_2 phase is only visible upon cooling. The inclusions homogenize mainly to the liquid phase, but also to the vapor at temperatures ranging 260°–323 °C (Fig. 2). Melting temperatures of ice are between −1.0° and −2.5 °C.

Table 2. Main types of fluid inclusions with their microthermometric features. L, aqueous solution; V, vapor phase; S, solid inclusion; Tm, temperature of final melting (°C) of CO_2 (CO_2 solid), i (ice); TH (temperature of homogenization, °C) of CO_2 (CO_2 liquid or vapor); homogenization phase means global homogenization of the inclusion

Inclusion types	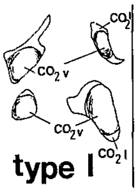	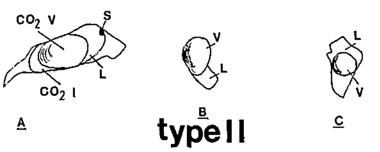			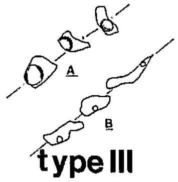		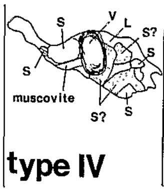	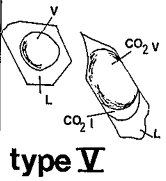
Subtypes		IIA	IIB	IIC	IIIA	IIIB	S	
Size µm	12 to 15	10 to 50	10 to 20	20 to 30	10 to 55	5 to 60	25 to 75	25 to 180
Degree of inclusion filling at 25 °C %	50 to 100	50 to 70	40 to 70	50 to 70	40 to 70	< 30	10 to 30	20 to 70
Tm CO_2 °C	− 56.6 to − 58.0	− 56.7 to − 57.5	− 56.9 to − 58.5	–	–	–	–	−56.6 to −57.1
Tm C °C	–	+ 6.0 to + 8.0	+ 9.5 to + 10.0	+ 7.8 to + 9.0	–	–	–	+ 3 to + 8.5
TH CO_2 °C	Liq: + 16.8 Vap: + 28 to + 30	+ 21.4 to + 29.0 in Vapor phase	–	–	–	–	–	+ 15.5 to 27.2 in vapor phase
Tm_i °C	–	− 1.4 to − 4.0	− 1.0 to − 2.5	− 1.3 to − 5.0	− 0.5 to − 6.5	− 0.1 to − 7.0	− 0.5 to − 6.5	− 1 to − 8.9
TH °C	–	+ 300 to + 370	+ 260 to + 323	+ 220 to + 420	+ 270 to + 400	+ 100 to + 280	+ 150 to + 210	+ 180 to + 340
Homogenization phase	–	Vapor and liquid	Liquid vapor critical	Liquid sometimes vapor	Liquid sometimes vapor	Liquid	Liquid	Liquid

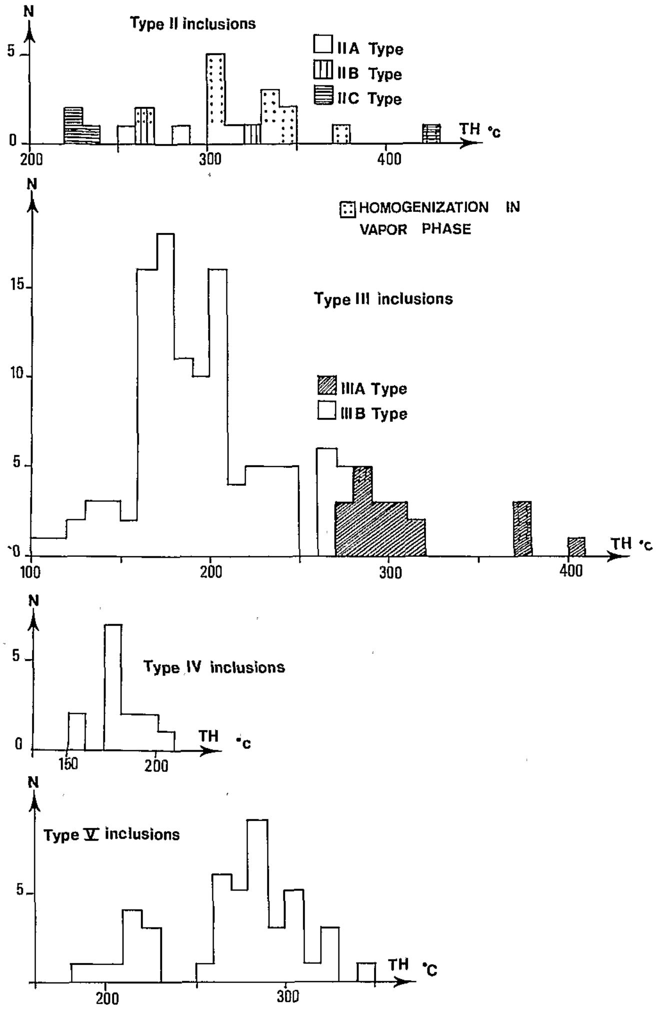

Fig. 2. Histograms of fluid-inclusion homogenization temperature from Xihuashan quartz veins. TH, temperature of homogenization; N, number of measurements

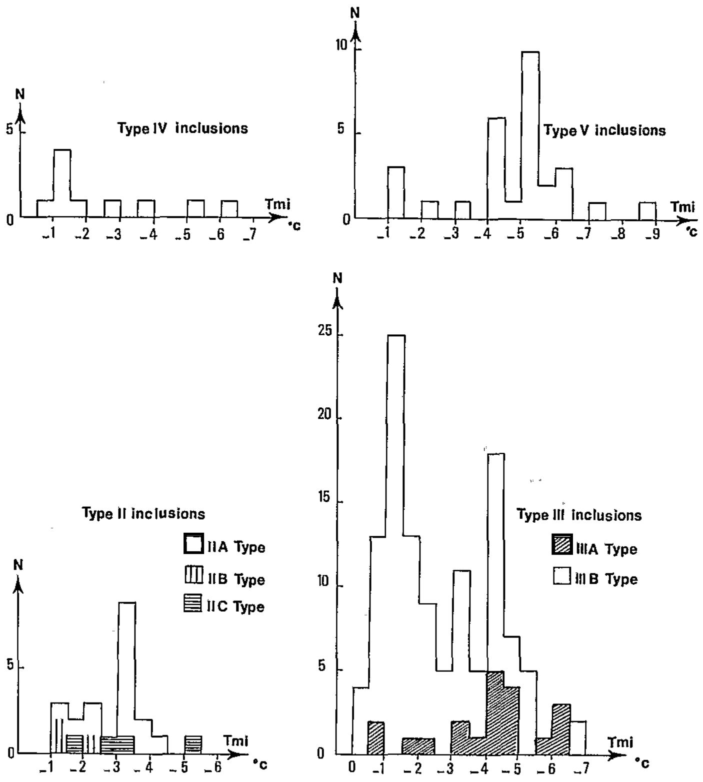

Fig. 3. Histograms of fluid-inclusion melting temperature of ice from Xihuashan quartz veins. Tmi, melting temperature of ice; N, number of measurements

Type-IIC inclusions have a complex shape and are 20–30 μm in size. They are isolated in quartz or occur along healed fracture planes. In most inclusions, the liquid phase occupies 30%–50% of the total volume and, at moderate temperatures the occurrence of CO_2 is indicated by the formation of a solid phase considered to be CO_2 clathrate ($CO_2 \cdot 5\frac{3}{4} H_2O$) due to its melting temperature of between 7.8° and 9.0 °C. Homogenization temperatures are scattered between 220° and 420 °C. Homogenization occurs in liquid and sometimes in vapor; melting temperatures of ice are widely scattered between −1.3° and −5.0 °C (Fig. 3).

H_2O type (type III). These inclusions are the most abundant in all samples. They occur along secondary healed fracture planes that riddle the quartz. They belong to early and late fluid circulations and testify to successive microfracturing and superposition of hydrothermal events. Based on variations in shape, gas/liquid filling ratio, and mainly on microthermometric features, two subtypes are distinguished, i.e., type IIIA, the earliest inclusions, and type IIIB, the latest inclusions.

Type-IIIA inclusions are generally simple or tabular in shape or are negative crystals; the walls of the inclusions are thick with some swellings. Their size is variable (10–55 μm), and the volume of the gas bubble comprises 40%–70% of the total inclusion. Melting temperatures of ice are scattered between −0.5° and −6.5 °C (Fig. 3). On heating type-IIIA inclusions homogenize to liquid at temperatures ranging 270°–400 °C and to vapor ranging 300°–380 °C.

Type-IIIB inclusions are extremely abundant; they have irregular shapes, but very often exhibit necking-down phenomena; their size ranges from several microns to 60 μm and the volume of the gas phase is generally small (less than 30% of the total inclusion). Melting temperatures of ice fall between −0.1° and −7 °C (Fig. 3), and they homogenize to liquid between 100° and 280 °C (Fig. 2).

Multiphase solid inclusions (type IV). This type is present in quartz from every level of the mine. They contain an aqueous phase (10–30 vol% of the total inclusion) and one or several solids. They are distributed along fracture planes and belong to the latest fluid generations. Their shape is very complex (Table 2) and size is variable (25–75 μm). Melting temperatures of ice range from −0.5° to −6.5°C (Fig. 3), and homogenization temperatures from +150° to +210 °C. Multiphase solid inclusions contain several solid phases that remain unchanged during heating: some inclusions show two or three mineral types, i.e., one without definite shape, white or pink in color, translucent, and anisotropic; a second solid phase with a lamellar or pseudohexagonal habit and yellow or white color like micas; and a fibrous, black solid phase with low refringence and isotropy.

H_2O-CO_2 type (type V). This type of inclusion is found in the idiomorphic drusy quartz from each level of the mine. They occur along growth zones or crystal faces; these primary inclusions are quite large (25–180 μm) with a negative crystal shape. At room temperature, Type V are two- or three-phase inclusions with the volume of the gas phase comprising between 20% and 70% of the total inclusion. Table 2 summarizes the microthermometric features; the melting temperatures of ice (Fig. 3) show a bimodal distribution (–4.2° and –5.2 °C) and their homogenization temperatures in the liquid phase are between 180° and 340 °C.

Electron microscopy

This technique allows the morphology of the inclusion cavity and the nature of the solid minerals to be determined. The experiment has been done on massive quartz, idiomorphic drusy quartz, and wolframite crystals.

Massive quartz. At first, the observations show the intense fracturing that affects the massive quartz clearly indicated by the occurrence of numerous healed microfractures and inclusion cavity linings; the different solid phases encountered in the cavities are muscovite, quartz, chlorite, Fe and Mn oxides, wolframite, and biotite. Multiphase solid inclusions show lamellar muscovite, Fe and Mn oxides, crystals of quartz, and complex compounds of Si, KCl, and Ca. Solid inclusions of wolframite are found in regular-shaped inclusions whose size ranges 3–26 μm (samples X632-8, X594-12); the crystals show two kinds of morphology, i.e., xenomorphic around 1 μm in size and subautomorphic with a prismatic form up to 2 μm in size. These crystals of wolframite coexist with clusters of muscovite.

Idiomorphic drusy quartz. The solid inclusions are muscovite, chlorite, biotite, lamellar quartz, and scheelite. In some samples, complex solid phases (Na, K, Cl, minor S) formed by the evaporation of the liquid released during inclusion opening can be also observed.

Wolframite crystals. Their analysis shows the scarcity of fluid inclusion cavity, their small size (4 μm), and the lack of solid inclusions.

Raman spectrometry

Analyses of the gaseous part of the inclusions have been performed with the Raman microprobe type M.O.L.E. The results for inclusion types I, II A, II B, and V are shown in Tables 3 and 4. The main constituent is CO_2 with a minor amount of N_2 and CH_4. Nonmeasurable traces of CO_2 have been detected in type III B.

Results and discussion

Qualitative and quantitative variations in the bulk composition of the fluids have been determined.

H_2O-CO_2-CH_4-N_2 inclusions. The $TmCO_2$-TmC diagram (Fig. 4) shows a negative correlation between type-II A and -II B inclusions which is consistent with the evolution marked by the increase in volatile components such as CH_4 and N_2 for a constant salinity (Fig. 5). The results indicate a decrease in CO_2 content and an increase in others volatiles and water.

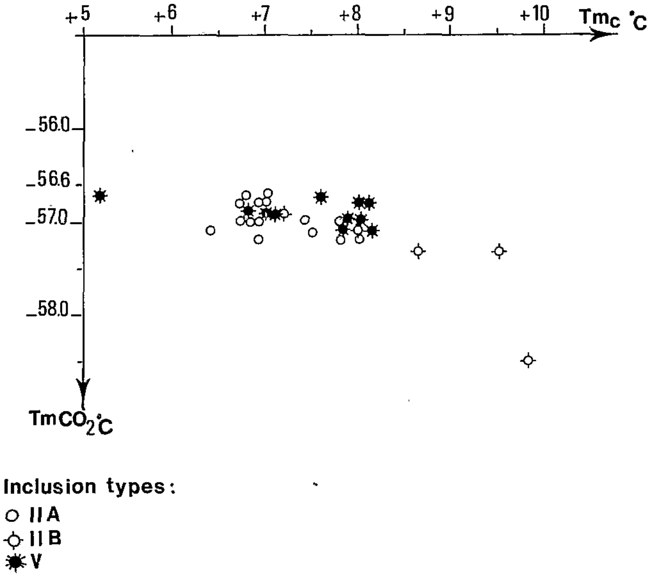

Fig. 4. TmC-$TmCO_2$ diagram of fluid inclusions from Xihuashan quartz veins. TmC, melting temperature of clathrate; $TmCO_2$, melting temperature of CO_2

The Th-Tmi diagram (Fig. 5) shows that the domain of type-V inclusions is quite different from that of type-II A inclusions. Type-V inclusions in idiomorphic drusy quartz appear similar to the type II A in morphology and microthermometric features ($TmCO_2$, TmC, $THCO_2$), but they differ in their degree of infilling (20 vol% < D.F. < 70 vol% of the inclusion), their higher salinity, and their homogenization in liquid; they apparently characterize the circulation of a second CO_2-bearing aqueous solutions and can not be considered contemporaneous to type-II A inclusions (Giuliani 1985). The pressure determination and the PVTX evolution for these carbonic fluids (CO_2-CH_4-N_2-H_2O-NaCl) are very complex. Considering type-II A inclusions containing 25 mol% CO_2, the equilibrium $L+V \rightleftharpoons V$ is reached for 300 °C at 550 bars (Takenouchy and Kennedy 1964): this value fixes the thermobarometric conditions of the equilibrium $L+V \rightleftharpoons V$, and so the minimum PT conditions for trapping type-II A inclusions. This value can be considered an approximation because the amounts of salts calculated are estimated, and the effects of CH_4 and N_2 are not taken in account.

H_2O-NaCl inclusions. Homogenization temperatures are shown in the Th-Tmi diagram (Fig. 5) showing the complex evolution of Xihuashan fluid inclusions.

–TH < 270 °C. This range of temperatures is mainly related to types III B and IV which are late aqueous inclusions. The scattering of values from type III B illustrates clearly the complexity of the hydrothermal evolution, affected by successive fracturating and fluid circulation. The Th-Tmi diagram shows for type IV a negative correlation: this variation in salinity related to short intervals of temperatures may result from dilution process.

–TH > 270 °C. Type-III A inclusions homogenize in the liquid or vapor phase at 270°–420 °C. Raman probe studies have detected no traces of CO_2 or other volatile phases. They are typically aqueous, low-density fluids (2–3 equiv. wt% NaCl). These observations indicate the presence of an early fluid that probably corresponds to a specific, high-temperature hydrothermal event. The inclusions which homogenize in the vapor phase are contemporaneous with those that homogenize into liquid

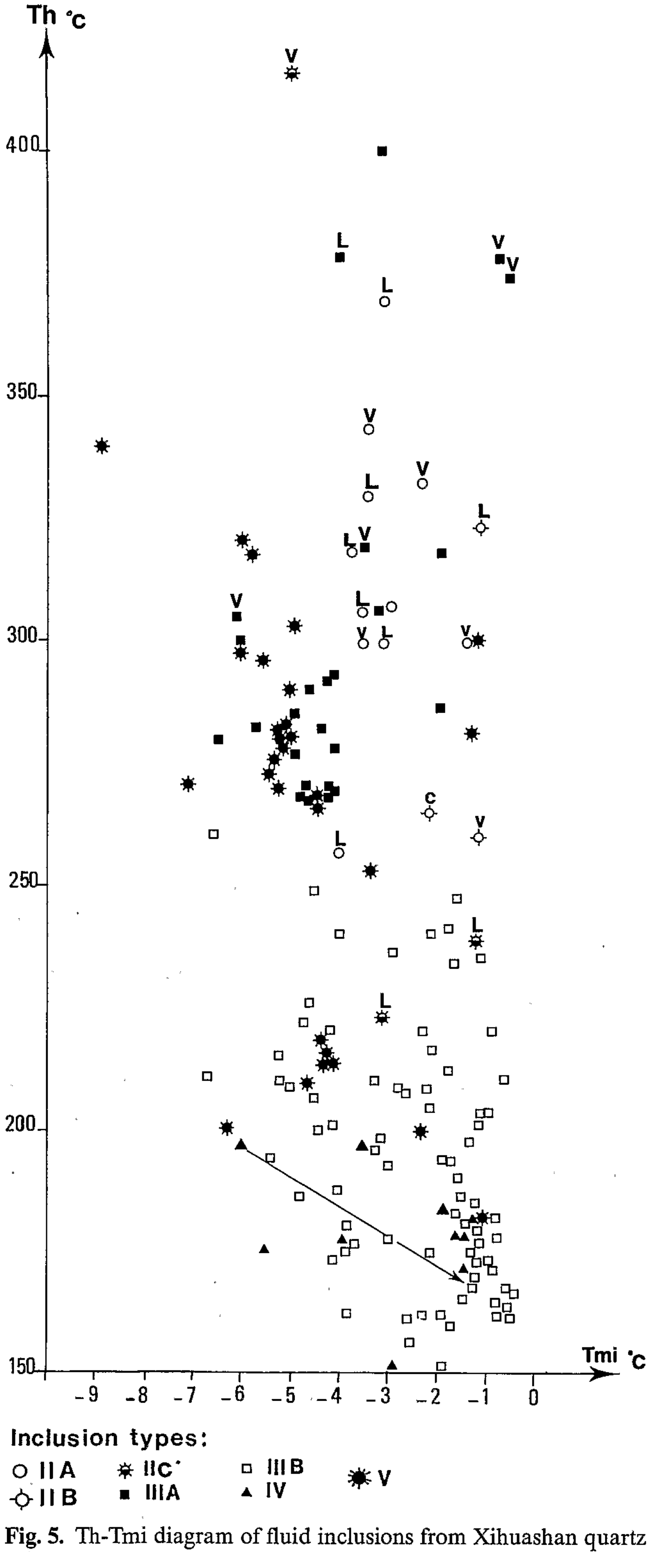

Fig. 5. Th-Tmi diagram of fluid inclusions from Xihuashan quartz veins. Th, temperature of homogenization; Tmi, melting temperature of ice; L, liquid homogenization; V, vapor homogenization; C, Critic homogenization; → Evolution of type IV inclusions

(between 310° and 380 °C). These observations can indicate unmixing of the fluid, although the respective salinities of these inclusions are close to each other so that the unmixing phenomenon must have been quite limited. Unmixing of the fluid appears evident at 380 °C (100–200 bars) and is characterized by an a aqueous solution of high salinity and a vapor of lower salinity (Fig. 5). This local boiling is not expressed systematically and is probably of minor importance in the evolution of the hydrothermal system. Below 300 °C, type-IIIA inclusions homogenize only to the liquid phase, and Tmi values lie between –4° and –7 °C. It appears that for temperatures near 300 °C, type IIIA is more saline (average of 7 equiv. wt% NaCl).

Fluid composition. The main features of the evolution of the chemical composition of the fluids can be summarized as shown in Fig. 6. During the whole process, the amounts of CO_2, CH_4, and N_2 do not change significantly, except in type-V inclusions (Fig. 6 A) which have higher salinity and lower carbon content (Fig. 6 B). The $CO_2(CH_4+N_2)$-NaCl-H_2O composition diagram (Fig. 6 C) shows the discontinuity between CO_2-rich inclusions (type I), aqueous inclusions (type IIIA), and H_2O-CO_2 inclusions (type IIA, IIB, V). The CO_2-rich inclusions contain CH_4 and N_2 in the same range as type IIA; the densest of these inclusions homogenizes in the liquid phase at 16.8 °C corresponding to an equivalent density of 0.8 g/cm^3. The presence of these inclusions, in which no water meniscus is visible, is surprising in such a geological environment. However, the presence of an undetected meniscus smaller than 1 μm can imply a water filling of 50%, and so the characterization of this type of inclusion is very imprecise, and it may belong to the CO_2-H_2O type.

Presence of nitrogen. The Raman microprobe demonstrates the presence of small amounts of nitrogen in Xihuashan fluid inclusions. Roedder (1972) summarized data on nitrogen in fluid inclusions, but the recent use of the Raman technique very often shows the presence of this gas in inclusions from various environments: metamorphic rocks (Dhamelincourt et al. 1979; Kreulen and Schuiling 1981), olivine crystals (Massare et al. 1980), dolomite and quartz from Tunisia (Guilhaumou et al. 1981), and also hydrothermal tungsten-bearing quartz veins from central Morocco (Cheilletz 1984; Giuliani 1984; Bennani and Weisbrod 1985). In the tungsten deposits under discussion, the amount of nitrogen can reach 5 mol% (Giuliani 1984) whose source is not well explained. Kreulen and Schuiling (1981) considered three possibilities, i.e., 1) the breakdown of organic matter, 2) the breakdown of K-silicate mineral (biotite, K-feldspar) where NH_4^+ substitutes K^+, and 3) a deep origin by the concentration of N_2 in the gaseous phase.

N_2-rich inclusions have been observed in quartz from black shales submitted to contact metamorphism in several localities (Bastoul 1983). N_2 appears to be most probably released from micas and feldspars during the metamorphism. During the diagenesis of organic-bearing sediments, nitrogen is stored in these minerals and can be liberated at high temperature (Kreulen and Schuiling 1981; Dubessy and Ramboz 1986). As black shales represent the enclosing rocks of the Xihushan granite, a similar origin is proposed.

Conclusions

The fluid inclusion study of the Xihuashan tungsten deposit shows that the hydrothermal quartz veins contain aqueous and CO_2-bearing inclusions which homogenize

Table 3. Microthermometric and Raman results for representative types of inclusions from Xihuashan quartz veins. dfw, degree of filling of the inclusion at room temperature (volumetric fraction of the aqueous liquid in the inclusion); dfc, degree of filling of the nonaqueous part of the inclusion (carbon-rich liquid + carbon-rich gas); Tm (temperature of final melting, °C) of CO_2 (CO_2 solid), i (ice), c (chlatrate); TH (temperature of homogenization, °C) of CO_2 liquid (L) or vapor (V); TD, temperature of decrepitation; XCO_2, and XCH_4 are given in molar fractions

Type of inclusion and sample		dfw	dfc	Microthermometry						Raman spectroscopy		
				$TmCO_2$	Tmi	Tmc	$THCO_2$	TH	TD	XCO_2	XN_2	XCH_4
I	X594-12 B1-11		1: 0.5 L 0.5 G	−57.5			+16.8 L			96.9	2.8	0.3
	X594-12 B1-15		1: 0.3 L 0.7 G	−57.0			+28.5 G			98.9	0.9	0.2
IIA	X632-3B A1-1	0.3	0.7	−56.7	−1.4	+7.0	+26.0 G	+300 V	300	97.8	2.2	–
	X632-3B A5-2	0.3	0.7	−57.1	−3.5	+6.4	+27.0 G	+300 V	310	99.5	0.3	0.2
	X594-12 B1-7	0.4	0.6	−57.0	−3.0	+6.7	+28.2 G	+307 V	360	99.8	–	0.2
	X594-12 B1-21	0.2	0.8	−56.8	−2.5	+8.0	+28.0 G	+340 V		100.0	–	–
IIB	X431-6 C1	0.3	0.7	−57.3	−1.2	+9.5	–	+260 V		93.6	2.3	4.1
	X431-6 C2	0.4	0.6	−57.5	−2.1	+9.8	–	+265 V		93.7	4.1	2.2
V	X594-12 H1	0.4	0.6	−56.7	−5.5	+5.2	+19.1 V	+270 L		96.3	2.8	0.9
	X594-12 F1	0.6	0.4	−56.8	−5.1	+8.0	+16.0 V	+280 L		97.6	1.4	1.0
	X594-12 G1	0.4	0.6	−56.9	−4.9	+7.2	+15.5 V	+303 L		96.0	3.4	0.6

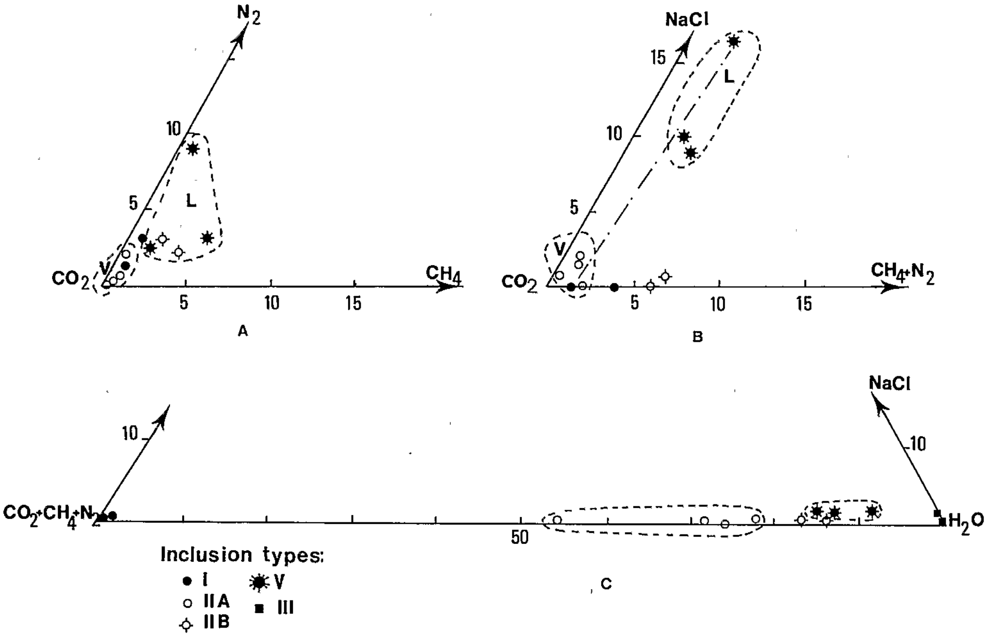

Fig. 6A–C. Composition and evolution of fluid inclusions from the mineralized quartz veins of Xihuashan for the *A* N_2–CO_2–CH_4, *B* NaCl–CO_2–CH_4 + N_2, and NaCl–CO_2 + CH_4 + N_2–H_2O systems; L, liquid inclusions; V, vapor inclusions

Table 4. Bulk composition for representative types of inclusions from Xihuashan quartz veins. X eq. CH_4, XCH_4+XN_2; $\bar{v}$, molar volume (cm^3 and $mole^{-1}$); ds, bulk density of the inclusion ($g\ cm^{-3}$); XH_2O, XCO_2, XCH_4, XN_2, and XNaCl in bulk composition (mol%)

Type of inclusion and sample		Salinities XNaCl (moles %)	X eq. CH_4 $\times 10^{-2}$	$\bar{v}$	ds	XH_2O	XCO_2	XCH_4 (moles %)	XN_2	XNaCl
I	X594-12 B1-11				0.8		96.9	0.3	2.8	
	X594-12 B1-15				0.3		98.9	0.1	1.0	
IIA	X632-3B A1-1	0.75	2.18	130	0.53	73.3	26.2	–	0.5	–
	X632-3B A5-2	1.72	0.47	120	0.55	71.7	27.8	–	–	0.5
	X594-12 B1-7	1.60	0.18	110	0.64	77.8	21.7	–	–	0.5
	X594-12 B1-21	1.33	0.00	90	0.59	54.2	45.6	–	–	0.2
IIB	X431-6 C1	0.64	6.36	240	0.42	83.2	15.9	0.6	0.3	–
	X431-6 C2	1.12	6.24	220	0.52	86.7	12.3	0.3	0.4	0.3
V	X594-12 H1	2.81	3.68	195	0.54	84.9	13.3	0.1	0.3	1.4
	X594-12 G1	2.53	4.0	225	0.53	86.2	11.9	0.6	0.3	1.4
	X594-12 F1	2.62	2.42	225	0.69	91.6	6.8	–	0.6	1.5

into the liquid or vapor phase between 150° and 420 °C with salinities of 1–10 equiv. wt% NaCl. These results agree with the work of Lu et al. (1982) who found similar microthermometric features in ten hydrothermal veins from tungsten ore deposits in southern China.

The hydrothermal evolution results from a complex fluid circulation corresponding to successive fluid generations with variable compositions and pressures and temperatures of trapping. These successive fluid generations are responsible for discontinuous events during the continuous cooling of the hydrothermal system. There are two types of earlier fluids, i.e., low-salinity, low-density CO_2-bearing aqueous solutions circulating at temperatures up to 420 °C, and low-salinity (2–3 equiv. wt% NaCl) CO_2-free aqueous solutions circulating at temperatures from 280° up to 400 °C, which correspond to a specific hydrothermal event; local and limited unmixing phenomena may occur at 380 °C and 200–100 bar, probably in response to a sudden pressure drop. The fluids contemporaneous with the idiomorphic drusy quartz are typically pure CO_2-bearing aqueous solutions of low salinity (2.5 equiv. wt% NaCl), homogenizing at low to moderate temperatures (180°–340 °C). The hydrothermal evolution ends with cooler fluids of variable salinities which homogenize in the liquid phase between 100° and 275 °C.

Many fluid inclusion studies from tungsten vein deposits show that complex carbonic fluids might play an important role in the transport and deposition of tungsten in hydrothermal systems (Kalyuzhni et al. 1975; Naumov and Ivanova 1971; Higgins 1980; Ramboz 1980; Ramboz et al. 1985). The precipitation of the tungsten is favored by different mechanisms such as unmixing of of an homogeneous solution into two different fluids (Higgins 1980; Ramboz et al. 1982) or mixing of two fluids of different compositions (Giuliani 1984; Ramboz et al. 1985). In other tungsten deposits, fluid inclusion studies only indicate the presence of aqueous fluids enriched in chloride with no significant concentrations of CO_2 (Jackson et al. 1977, Charoy 1979; Bazheyev 1980; Bray 1980).

In the case of the Xihuashan tungsten deposit, the importance assigned to the carbonic fluid inclusions which are the least-abundant type found in the quartz, and the role played by the CO_2-rich fluids in the transport of tungsten can be discussed. The typical tungsten-bearing quartz vein from the southern Jiangxi province shows a pronounced vertical zonation containing ore-rich shoots of very high grade wolframite ore in a restricted vertical extent. This ore shoot passes downward into low-grade, sulfide-rich ore. This zonation is well illustrated by vein 2.99 where the sudden stop of the economic zone is exactly 10 m up level 538 and marked by the precipitation of molybdenite, bismuthinite, and others sulfides. No important mixing of fluids or unmixing of a homogeneous solution was checked to explain this vertical zonation. Meanwhile, we can observe that the earliest CO_2-H_2O fluids from the hydrothermal system are present especially in levels 632 and 594 and associated with the minerals from the oxide stage specially wolframite. These carbonic fluids are also encountered (type-V inclusions) in the late drusy quartz generally related to the sulfide stage and thus reflect their circulation during the entire hydrothermal system evolution.

The aqueous fluid inclusions are present in all levels and always possess a secondary character. They are high- (type-III A inclusions) or low- (type-III B inclusions) temperature fluids probably formed in the gradual and systematic cooling of the ore fluids. The results of fluid inclusion study show that there is no important or anomalous reversals in depositional temperatures, fluid salinities, or fluid composition. They support the model of the circulation of successive fluid generations during a continuous cooling of the hydrothermal system. In this schema, it is difficult to define exactly the ore-forming fluids responsible for tungsten deposition. Meanwhile, it appears that the earlier carbonic fluids (type-II inclusions), mainly associated with the oxide stage, may have played a role in the transport and deposition of tungsten.

Additional sampling and fluid inclusion study from other veins at Xihuashan for the same levels or the study of a typical zoned deposit like Piaotang in the same mining district would bring more information on the association of tungsten deposits with these CO_2-rich hydrothermal fluids.

Acknowledgments. This work was done at the GIS/BRGM, Orléans (France), in 1982. The author is grateful to Cl. Ramboz and A. Cheilletz (Centre de Recherches Pétrographiques et Géochimiques de Nancy) and also M. Cuney (C.R.E.G.U.) for their suggestions and corrections of this manuscript and to Ian Mc. Reath (Bahia Federal University, Brazil) for his help with the English translation. Raman spectrometric analyses were done at the C.R.E.G.U. laboratory (Nancy, France) by Dr. J. C. Kostolanyi.

References

Arai, Y., Kaminshi, G., Saito, S.: The experimental determination of the P-V-T-X relations for the carbon dioxide-nitrogen and the carbon dioxide-methane systems. J. Chem. Eng. Japan 4: 113–122 (1971)

Bastoul, A.: Etude des fluides carbo-azotés associés au metamorphisme de contact des schistes noirs sur l'exemple des Jebilets centrales (Maroc). Comparaison avec la région des Bondons et de Penaran (France). Thése 3° cycle, Institut National Polytechnique de Nancy, 189 p. (1983)

Bazheyev, Ye. D.: Evolution of hydrothermal solutions during the formation of tungsten deposits (for the case of Soktuy ore Lode). Geokhimiya 10: 1461–1467 (1980)

Bennani, M., Weisbrod, A.: Chimie des fluides hydrothermaux et minéralisations Sn-W dans les secteurs de Tarmilat Zgit (Sud du district de Walmès), Maroc Central. Bull. Serv. Geol. Maroc (in press) (1985)

Bozzo, A.T., Chen, H.S., Kass, J.R., Barduhn, A.J.: The properties of the hydrates of chlorine and carbon dioxide. Inter. Symposium on Fresh Water from the Sea 3:437–451 (1973)

Bray, C.J.: Mineralization, greisenisation and kaolinisation at Goonbarrow China Clay pit, Cornwall. U.K. Unpublished D. Phil. Thesis. Oxford (1980)

Burrus, R.C.: Analysis of fluid inclusions in graphitic metamorphic rocks from Bryand Pond, Maine and Khtada lake. British Columbia: thermodynamic basis and geologic interpretation of observed fluid compositions and molar volumes. Unpublished Ph.D. Thesis, Princeton University (1977)

Charoy, B.: Définition et importance des phénomènes deutériques et des phases fluides associées dans les granites; Conséquences métallogéniques. Sci. de la Terre, France 37: 364 p. (1979)

Cheilletz, A.: Caractéristiques géochimiques et thermobarométriques des fluides associés à la scheelite et au quartz des minéralisations tungstifères du Djebel Aouam (Maroc Central). Bull. Minéral. 107:255–272 (1984)

Delhaye, M., Dhamelincourt, P.: Raman microprobe and microscope with laser excitation. Jour. Raman Spectrosc. 3:33–43 (1975)

Dhamelincourt, P., Beny, J.M., Dubessy, J., Poty, B.: Analyse d'inclusions fluides à la microsonde Mole à effet Raman. Bull. Minéral. 102:600–610 (1979)

Donelly, H.G., Katz, D.L.: Phase equilibria in carbon dioxide methane system. Industr. Engng. Chem. 46:511–517 (1954)

Dubessy, J., Ramboz, Cl.: The history of organic nitrogen from early diagenesis to amphibolite facies: mineralogical, chemical, mechanical and isotopic implications. Abstract 5° Water Rock Interaction Congress, Irland (1986)

Ellis, A.J., Golding, R.M.: The solubility of carbon dioxide above 100 °C in water and in sodium chloride solutions. Amer. Jour. Sci. 261:47–60 (1963)

Giuliani, G.: Les concentrations filoniennes à tungstène-étain du massif granitique des Zaër (Maroc Central): Minéralisations et phases fluides associées. Mineral. Deposita 19:193–201 (1984)

Giuliani, G.: Le gisement de tungstène de Xihuashan (Sud-Jiangxi, Chine): relations granites, altérations deutériques-hydrothermales, minéralisations. Mineral. Deposita 20: 107–115 (1985)

Guilhaumou, N., Dhamelincourt, P., Touray, J.C., Touret, J.: Etude des inclusions fluides du système N_2-CO_2 de dolomites et de quartz de Tunisie septentrionale. Donnés de la microcryoscopie et de l'analyse à la microsonde à effet Raman. *Geochim. Cosmochim.* Acta 45:657–673 (1981)

Hepworth, J.V., Yu, H.Z. Editors: Tungsten geology, Jiangxi, China. 584 p. (1982)

Heyen, G., Ramboz, Cl., Dubessy, J.: Simulation des équilibres de phases dans le système CO_2-CH_4 en dessous de 50 °C et de 100 bars. Application aux inclusions fluides. C.R. Acad. Sci. Paris 294:203–206 (1982)

Higgins, N.C.: Fluid inclusion evidence for the transport of tungsten by carbonate complexes in hydrothermal solutions. Can. J Earth. Sci. 17:823–830 (1980)

Hsu, K.C.: Tungsten deposits of southern Kiangxi, China. Econ. Geol. 38:431–474 (1943)

Ishihara, S., Takenouchy, S. Editors: Granitic magmatism and related mineralizations. Mining Geol. Spec. Issue 8:247 p. (1980)

Jackson, N.J., Moore, J.McM., Rankin, A.H.: Fluid inclusions and mineralizations at Cligga Head, Cornwall, England. J. Geol. Soc. London 134:343–349 (1977)

Kalyuzhnyi, VL.A., Davidenko, N.M., Zinchuck, I.N., Svoren, I.M., Pisotskiy, B.I.: Role of CO_2-H_2O and CH_4-H_2O fluids in forming of ore of gold at Chukotka (Abstract). In: Fluid inclusion research 8: p. 82 (1975)

Kreulen, R., Schuiling, R.D.: N_2-CH_4-CO_2 fluids during formation of the Dôme de l'Agout, France. Geochim. Cosmochim. Acta 46:193–203 (1981)

Le Bel, L., Li, Y.D., Sheng, J.F.: Granitic evolution of the Xihuashan-Dangping tungsten-bearing systems (Jiangxi-China). Tschermaks Min. Petr. Mitt. 33:149–167 (1984)

Lu, H., Shi, J., Yu, C., Xu, S.: Geologic and fluid inclusion studies of ten types of tungsten ore deposits in South-China. Geochemistry, 1, 2:200–217 (1982)

Marujeol, P., Cuney, M.: Xihuashan W-bearing granites (Jiangxi-China): mineralogical controls on REE, Y, Th, U mobility during magmatic evolution and hydrothermal alteration. Terra Cognita, V. 5, 2–3, p. 284 Abstract (1985)

Massare, D., Chlocchiatti, R., Touret, J.: Fluides résiduels et minéraux réactionnels dans les olivines gemmes de l'île de Zebargard (Mer Rouge), signification pétrogénétique et tectonique. 8° RAST, p. 244 (1980)

Naumov, V.B., Ivanova, G.F.: The pressure and temperature conditions for formation of wolframite deposits. Geochim. Inter. 8:381–394 (1971)

Potter, R.W., Brown, D.L.: The volumetric properties of aqueous sodium chloride solutions from 0° to 500 °C at pressures up to 2,000 bars based on a regression of available data in the literature. Geol. Surv. Bull. USA 1421C:1–36 (1977)

Potter, R.W., Clynne, M.A., Brown, D.L.: Freezing point depression of aqueous sodium chloride solutions. Econ. Geol. 73: 284–285 (1978)

Poty, B., Stalder, T., Weisbrod, A.: Fluid inclusions studies in quartz from fissures of western and central Alps. Schweiz. Mineral. Petrogr. Mitt. 54:2/3, 717–752 (1974)

Poty, B., Leroy, J., Jachimowicz, L.: Un nouvel appareil pour la mesure des températures sous le microscope: l'installation de microthermométrie Chaixméca. Bull. Soc. Fr. Min. Cristall. 99:182–186 (1976)

Ramboz, Cl.: Géochimie et étude des phases fluides des gisements et indices d'étain-tungstène du sud du Massif Central (France). Thèse 3° Cycle INPL Nancy 278 p. (1980)

Ramboz, Cl., Pichavant, M., Weisbrod, A.: Fluid immiscibility in natural processes: use and misuse of fluid inclusion data. II. In: Chem. Geol. 37:29–48 (1982)

Ramboz, Cl., Schnapper, D., Dubessy, J.: The P-$\bar{V}$-T-X-fO_2 evolution of H_2O-CO_2-CH_4-bearing fluid in a wolframite vein: Reconstruction from fluid inclusion studies. Geochim. Cosmochim. Acta. 49:205–219 (1985)

Roedder, E.: Compositions of fluid inclusions. In: Data of geochemistry. Editor Fleischer, M. U.S. Geol. Surv. Professional Paper, 440-JJ, 164 p. (1972)

Sarashina, E., Arai, Y., Saito, S.: Vapor liquid, equilibria for the nitrogen, methane, carbon dioxide system. J. Chem. Eng. Japan 4:377–378 (1971)

Schrötter, H.W., Klöckner, H.W.: Raman scattering cross section in gases and liquids. In: Raman Spectroscopy of gases and liquids. Ed. Weber. 4:123–166, Berlin-Heidelberg-New York: Springer 1979

Takenouchy, S., Kennedy, G.C.: The binary system H_2O-CO_2 at high temperatures and pressures. Amer. Jour. Sci. 262: 1055–1074 (1964)

Tanelli, G.: Geological setting, mineralogy and genesis of tungsten mineralization in Dayu district, Jiangxi: an outline. Mineral. Deposita 17:279–294 (1982)

Touret, J.: The significance of fluid inclusions in metamorphic rocks in thermodynamics in geology. Nato advanced study institutes series, Series C, Donall G., Fraser Editors, 203–227 (1976)

Wang, Z., Zhao, Z., Zhao, H.: Ree distribution patterns of granites in South China. Geochemistry 1:39–50 (1982)

Wang, Ch.: Geochemistry of vein-type tungsten deposits in South Jiangxi. Min. Deposits 3:76–84, Beijing (1984)

Wu, Y.L., Mei, Y.W.: Multi-phase intrusion and multi-phase mineralization and their evolution in Xihuashan tungsten ore field. In: Tungsten Geology Symposium, Jiangxi, China. ESCAP-RMRDC, Bandung, 437–449 (1982)

Yan, M.Z., Wu, Y.L., Li, C.Y.: Metallogenic systems of tungsten in South-East China and their mineralization characteristics. Granitic magmatism and related mineralization. Mineral. Geol. Spec. Issue 8: Japan, 215–221 (1980)

Ypma, P.: Rejuvenation of ore deposits as exemplified by the Belledone metalliferous province. Ph.D. Thesis, University Leiden (Holland) (1963)

Received: May 27, 1986
Accepted: June 25, 1987

Book review

Terence P. Scoffin: An introduction to carbonate sediments and rocks. Blackie & Son Ltd. Glasgow and London, 1987, 274 p. (in USA Chapman and Hall). Paperback DM 45.–, £ 12.00

Carbonate rocks in many aspects are challenging subjects of investigation for the economic geologist: a considerable part of the world's oil production originates from them, they are host rocks for lead, zinc, fluorite or barite, and other metallic and nonmetallic minerals, and not least, they represent a group of indispensable industrial rocks. The *Introduction to carbonate sediments and rocks,* as now presented by Terence Scoffin, may well provide the necessary basic knowledge when dealing with these fields.

The intention of the author was to prepare a book for the "advanced undergraduate geologist", which could be an introduction to the research-level books on carbonate rocks already available. Consequently, the book begins with a brief introduction to carbonate minerals, limestone classification, and definition of environmental and ecological terms. In part 2, skeletal and non-skeletal carbonate grains are described, and in part 3 an outline is given for the predominant marine depositional processes, i.e., sedimentation of carbonate grains and reef growth. Postdepositional changes are discussed for marine, meteoric, and deep-burial diagenetic settings in part 4, giving space, e.g., for trace element and isotopic changes during diagenesis, and the origin of dolomites. On this broad basis, conditions and products of modern and ancient carbonate depositional environments are presented in parts 5 and 6 of the book with a wealth of information. In particular the author deserves credit for adding a final chapter on some economic aspects of carbonate sediments and rocks to his book. Here he concentrates mainly on porosity characteristics and the distribution and geometry of the hydrocarbon reservoir rocks, but additionally gives some impressions of carbonate rocks as hosts of ore deposits, especially of the Mississippi Valley type.

Altogether, the book offers a very useful review of the most important aspects of carbonate sedimentology, well illustrated with a great number of examples. For all those who want to go to the bottom of the matter, a recommended reading list at the end of each chapter opens up this way, too. Anyone occasionally looking for concise and well-founded guidance in the field of carbonate sedimentology will appreciate this reasonably priced textbook.

K. Germann (Berlin)